REYNOLDS NUMBER DEPENDENCE OF A TURBULENT CHANNEL FLOW WITH ROUGHNESS ON ONE WALL.

S. Leonardi, P. Orlandi
Dipartimento di Meccanica e Aeronautica, University of Rome "La Sapienza", 00184, Rome, Italy

R. A. Antonia
Discipline of Mechanical Engineering, University of Newcastle, NSW 2308 Australia

ABSTRACT

Direct Numerical Simulations of turbulent channel flow with square bars on the bottom wall are discussed have been carried out at different Reynolds numbers. The results tend to confirm the inappropriateness of the roughness function as an indication of the effect a particular roughness geometry exerts on the flow. Distributions of turbulent intensities support the improvement in global isotropy relative to a smooth–wall.

INTRODUCTION

Flows over rough surfaces are of interest in many practical applications, ranging from shipbuilding and aviation, the flows over blades in different types of turbomachines and the flows over vegetated surfaces in the atmospheric surface layer. In all these cases, the Reynolds number is high and the roughness is very small relative to the characteristic length of the outer flow. Direct numerical simulations (Leonardi *et al.* 2003, Ashrafian *et al.* 2004) and LES, (Cui *et al.* 2003) have been carried out for only one Reynolds number and have not addressed the Reynolds number dependence. In the present paper, we discuss direct numerical simulations of turbulent channel flows with roughness on the lower wall at different Reynolds numbers. The aim is to clarify how the near-wall structures and statistics depend on the Reynolds number. If the dependence is weak, DNS can be useful to understand the physics of real turbulent rough flows. Moreover, DNS results can be used to develop new sub–grid models or closures for RANS.

We consider a fully developed turbulent channel flow with square bars on the bottom wall. Two values $(1, 9)$ for w/k (w is the spacing between roughness elements and k is the roughness height) are discussed. Periodic boundary conditions apply in the streamwise (x_1) and spanwise (x_3) directions respectively. DNSs have been carried out at $Re = U_c h/\nu = 4200$, 10400 and 18000, U_c is the centerline velocity, h the half–width of the channel and ν is the kinematic viscosity. For the smooth–channel, $h^+ = 180$ and 380 for $Re = 4200$ and 10400 respectively. The computational box is $8h \times 2.1h \times \pi h$ in x_1,x_2 and x_3 respectively. The additional $0.1h$ increase in the channel height is due to the cavity height where the square elements are placed, $(k = 0.1h)$. The plane of the crests is at $x_2/h = -1$. The flow rate has been kept constant in all simulations. The flow can be assumed to be "fully rough" since k^+ ranges from about 20 for $w/k = 1$ to about 160 for $w/k = 9$ at the larger Reynolds number.

NUMERICAL PROCEDURE

The non-dimensional Navier-Stokes and continuity equations for incompressible flows are:

$$\frac{\partial U_i}{\partial t} + \frac{\partial U_i U_j}{\partial x_j} = -\frac{\partial P}{\partial x_i} + \frac{1}{Re}\frac{\partial^2 U_i}{\partial x_j^2} + \Pi\,, \qquad \nabla \cdot U = 0 \quad (1)$$

where $Re = (U_c h/\nu)$ is the Reynolds number, h is the channel half-width, U_c is the centreline velocity, ν is the kinematic viscosity, Π is the pressure gradient required to maintain a constant flow rate, U_i is the component of the velocity vector in the i direction and P is the pressure. The Navier-Stokes equations have been discretized in an orthogonal coordinate system using the staggered central second-order finite-difference approximation. Here, only the main features are recalled since details of the numerical method can be found in Orlandi (2000). The discretized system is advanced in time using a fractional-step method with viscous terms treated implicitly and convective terms explicitly. The large sparse matrix resulting from the implicit terms is inverted by an approximate factorisation technique. At each time step, the momentum equations are advanced with the pressure at the previous step, yielding an intermediate non-solenoidal velocity field. A scalar quantity Φ projects the non-solenoidal field onto a solenoidal one. A hybrid low-storage third-order Runge-Kutta scheme is used to advance the equations in time. The roughness is treated by the efficient immersed boundary technique described in detail by Fadlun *et al.* (2000). This approach allows the solution of flows over complex geometries without the need of computationally intensive body-fitted grids. It consists of imposing $U_i = 0$ on the body surface which does not necessarily coincide with the grid. Another condition is required to avoid that the geometry is described in a stepwise way. Fadlun *et al.* (2000) showed that second-order accuracy is achieved by evaluating the velocities at the closest point to the boundary using a linear interpolation. This is consistent with the presence of a linear mean velocity profile very near the boundary even for turbulent flows, albeit at the expense of clustering more points near the body.

MEAN FLOW

For $w/k = 1$ separation occurs at the trailing edge of the element and reattachment is on the opposite vertical wall (Leonardi *et al.* 2003). The cavity is filled by a stable vortex. For $w/k = 9$, the flow reattaches on the bottom wall. As the next element is approached, the streamlines are tilted

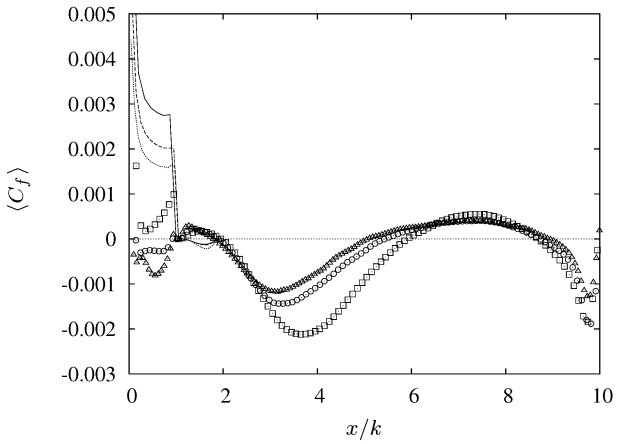

Figure 1: Normalised skin friction coefficient on the horizontal walls of a roughness element for $w/k = 1$ and $w/k = 9$. Symbols $w/k = 9$, lines $w/k = 1$. □ , ——— $Re = 4200$, ○ – – – – $Re = 10400$, △ ····· $Re = 18000$.

upward and a new separation region is formed. The skin friction coefficient exhibits a peak at the leading edge for both the geometries. Inside the cavity, the recirculation is very weak for $w/k = 1$, more intense for $w/k = 9$ (fig.1). By increasing the Reynolds number, for $w/k = 1$ the frictional drag decreases on the roughness crests plane. Within the cavity, the flow is so weak that appreciable effects cannot be observed. For $w/k = 9$, as the Reynolds number is increased, the reattachment on the bottom wall (first zero crossing) moves towards the trailing edge and the recirculation region becomes smaller; on the roughness crest plane at higher Reynolds number, the separation (negative friction) is more evident. The pressure along the walls is shown in figure 2

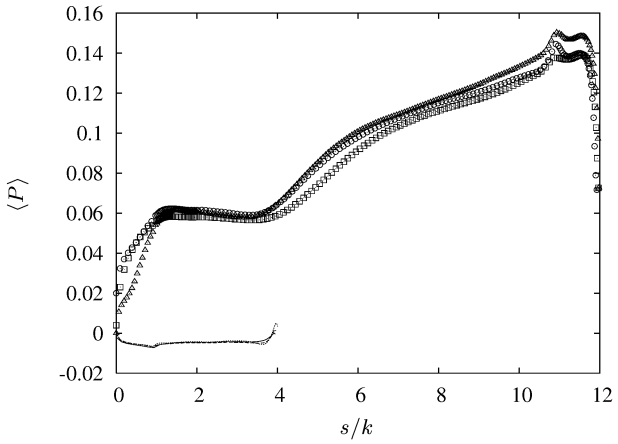

Figure 2: Pressure along the walls for one roughness wavelength (the coordinate s follows the walls of the cavity, the origin is at the leading edge). Legend as in fig.1.

over one roughness wavelength. As expected, the dependence on the Reynolds number is weaker than that for the frictional drag. For $w/k = 1$, the pressure is very low. Integrating the friction and pressure distribution along the wavelength the viscous ($\overline{C_f} = \lambda^{-1} \int_0^\lambda \langle C_f \rangle ds$) and form drag is obtained ($\overline{P_d} = \lambda^{-1} \int_0^\lambda \langle P \rangle \vec{n} \cdot \vec{x} ds$, $\vec{n}$ is the normal to the surface). For

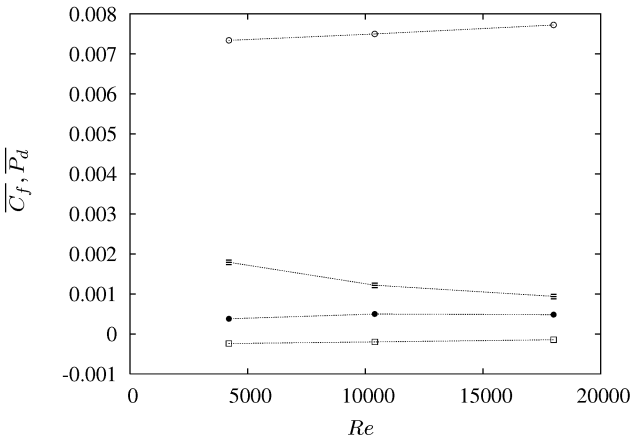

Figure 3: Dependence of frictional and form drag on the Reynolds number. □ frictional drag, ○ form drag. Empty symbols $w/k = 9$, filled $w/k = 1$.

$w/k = 1$, the viscous drag is the main contributor to the total drag, the form drag being negligible. The opposite occurs for $w/k = 9$. By increasing the Reynolds number, the form drag does not change much (for $w/k = 9$, it differs by about 5% from $Re = 4200$ to $Re = 18000$), while the viscous drag decreases appreciably (for $w/k = 1$ it changes by about 50% from $Re = 4200$ to $Re = 18000$). For $w/k = 9$, the viscous drag is negligible with respect to the form drag. The total drag and U_τ ($\equiv \sqrt{\overline{P_d} + \overline{C_f}}$) are almost independent on the Reynolds number. The opposite trend applies for $w/k = 1$ where both the total drag and U_τ change appreciably.

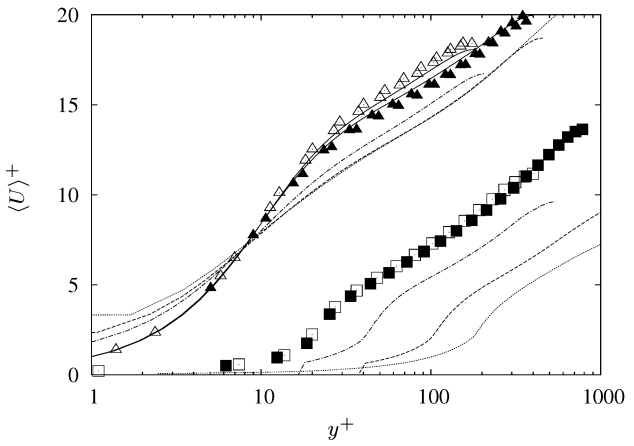

Figure 4: Mean velocity in wall units, solid lines Kim *et al.* $Re_\tau = 180$ and Moser *et al.* $Re_\tau = 395$. Symbols present simulations: △ smooth, □ $w/k = 3$; empty symbols $Re = 4200$, filled $Re = 10400$. For the smooth channel, profiles on both walls are shown; symbols are plotted every 4. Broken lines present simulations for $w/k = 1$ and $w/k = 9$ —·— $Re = 4200$, – – – – $Re = 10400$, ····· $Re = 10400$.

Direct Numerical Simulations allow U_τ ($\equiv \sqrt{\tau}$ where $\tau = \overline{P_d} + \overline{C_f}$) to be estimated reliably so that the mean velocity profile can be normalised properly by wall variables. It is usually assumed that the roughness affects the mean velocity in the logarithmic region through a shift ΔU^+, (roughness

function), such that

$$U^+ = \kappa^{-1} \ln\ y^+ + C - \Delta U^+ \ , \qquad (2)$$

where C and κ are constants and "+" denotes normalization by either U_τ or ν/U_τ. Perry *et al.* (1969) showed that, for $w/k > 1$, the roughness function depends on k^+ only, (k-type roughness), i.e.

$$\Delta U^+ = \kappa^{-1} \ln\ k^+ + B. \qquad (3)$$

This has been corroborated here by running two simulations for $w/k = 3$ at two different Re and k ($Re = 4200$, $k = 0.2h$ and $Re = 10400$, $k = 0.1h$) so as to have the same k^+. Since the mean velocity profiles in wall units overlap (figure 4), the results do not depend on Re and on the blockage due to the size of the elements (k/h). The independence of the results on k/h, for a given k^+, allows numericists to use larger elements and smaller Reynolds numbers with a lower computational cost. The velocity profiles are shown up to the location (y_{max}) of the maximum streamwise velocity, which does not coincide with the centreline but is shifted upward (Leonardi, Orlandi & Antonia 2005). In the same figure, results for the smooth channel at $Re = 4200$ and $Re = 10400$ are reported. There is a good agreement with those by Kim *et al.* (1987) and Moser *et al.* (1999). To gain further insight into the dependence of ΔU^+ with k^+, two sets of simulations have been performed, $w/k = 1$ and $w/k = 9$ for $Re = 4200, 10400$ and 18000. For $w/k = 9$, figure 3 shows that τ (and therefore U_τ) does not change. Usually, experimentalists determine the origin in y by fitting the mean velocity data to (2) after assuming a value of κ (usually 0.41). A more physical approach was proposed by Jackson (1981), who identified the origin in y with the centroid of the moment of forces acting on the elements. Both methods give an origin which does not change with the Reynolds number. The former gives an origin at $\epsilon/k = 0.9$ from the roughness crest plane, the latter at about $\epsilon/k = 0.53$. Here, the former assumption has been made to compare results with experiments; more details of the variation of ϵ/k with w/k can be found in Leonardi *et al.* (2003). Even if U_τ and ϵ/k do not change with Reynolds number, the downward shift of the velocity distribution for $Re = 18000$ is larger than that for $Re = 10400$ and 4200 (fig.4). This is in fact due to the increase of k^+ which is 80, 103 and 180 for $Re = 4200$, 10400 and $Re = 18000$ respectively. The corresponding values of ΔU^+ are 12.9, 13.5 and 14.8 respectively, in agreement with equation 3 and $B = 2.2$. For these values of k^+ we are in the fully rough regime (Bandyopadhyay 1987). The value of B depends on w/k, but varies only slightly in the range $3 < w/k < 9$. In fact, for $w/k = 7$ Bakken & Krogstad (2003) found experimentally a similar value of B ($B = 1.9$). If we take $y = \tilde{y} + \epsilon k$, where $\tilde{y}$ is the origin at the roughness crests plane, eq.2 can be rewritten as

$$U^+ = \kappa^{-1} \ln\ ((\tilde{y} + \epsilon k) U_\tau Re) + C - \Delta U^+ \ . \qquad (4)$$

The roughness function is therefore,

$$\Delta U^+ = -U^+ + \kappa^{-1} \ln\ ((\tilde{y} + \epsilon k) U_\tau Re) + C \ . \qquad (5)$$

U^+ varies slightly with Re (fig.5) then the roughness function varies mainly because of the term $\kappa^{-1} \ln\ (\tilde{y}^+ + \epsilon k^+)$ which is very similar to eq.3. In addition to eq.3, eq.5 shows that the dependence of ΔU^+ on k is only associated with the introduction of the shift in origin ϵ. If the y origin were at the roughness crest plane, i.e. $\epsilon = 0$, the log–region would not have a slope $\kappa = 0.41$ and the roughness function would not depend on k^+ even for $w/k = 9$ which is referred to as a "k–type" roughness. Then, the fact that the roughness function depends on k^+ is a consequence of how it is defined and, as such, does not have physical meaning. To further validate eq.5 we carried out 3 simulations for $w/k = 1$, $k/h = 0.1$ and $Re = 4200$, 10400, 18000. This geometry is called "d–type" roughness (Perry *et al.* 1969) to indicate that ΔU^+ does not depend on k^+. Figure 4 shows that the velocity distributions for $Re = 10400$ and $Re = 18000$ overlap, and that for $Re = 4200$ is only slightly different. To a close approximation, ΔU^+ does not depend on k^+; k^+ is 20, 43 and 67 for $Re = 4200$, 10400 and 18000 respectively. In this case, the origin in y is at the roughness crest plane so that $\epsilon = 0$. In fact equation 5 with $\epsilon = 0$ becomes independent of k^+. Even with the method of Jackson (1981), the origin in y is very close to the crests. Since for $w/k = 1$ the main contributor to the total drag is the friction, which acts on the roughness crest plane, the centroid of the moment is at $\epsilon = 0.05$. From these results, the classifications "d–type" and "k–type" roughness are only for to the different origins in y taken for the two types of geometries. The roughness function does not seem to represent a physical quantity which can describe the roughness. It is rather a mathematical quantity and its dependence on k^+ appears to be a consequence of how ΔU^+ is defined. To classify the large variety of rough walls we would need a more physical quantity than ΔU^+. Some work has been done in this direction. Suggestions have been made based on either the AIM (Smalley *et al.* 2002) or the wall–normal turbulent intensity Orlandi *et al.* (2003).

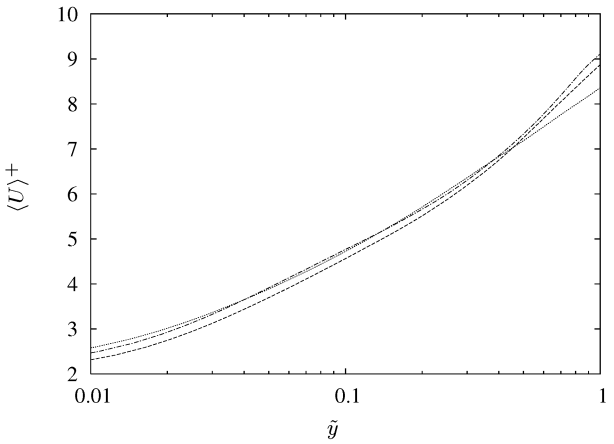

Figure 5: Mean velocity in wall units. The origin of $\tilde{y}$ is at the roughness crest plane. Broken lines present simulations for $w/k = 9$ — - - — $Re = 4200$, - - - - $Re = 10400$, ····· $Re = 10400$.

TURBULENT INTENSITIES

Turbulent intensities in wall units are shown in figure 6-8 for $w/k = 9$. The smooth wall distributions, included as reference, agree reasonably well with those by Kim *et al.* (1987) and Moser *et al.* (1999). Here, only the portion above the crest plane ($x_2/h = -1$) is shown. Despite an increase in $\langle u^2 \rangle$ (fig.7), $\langle u^2 \rangle^+$ is largely reduced consistently with the DNS by Bhaganagar, Kim & Coleman (2004) of a turbulent channel flow with 3D roughness on one wall. As expected, $\langle v^2 \rangle^+$ is

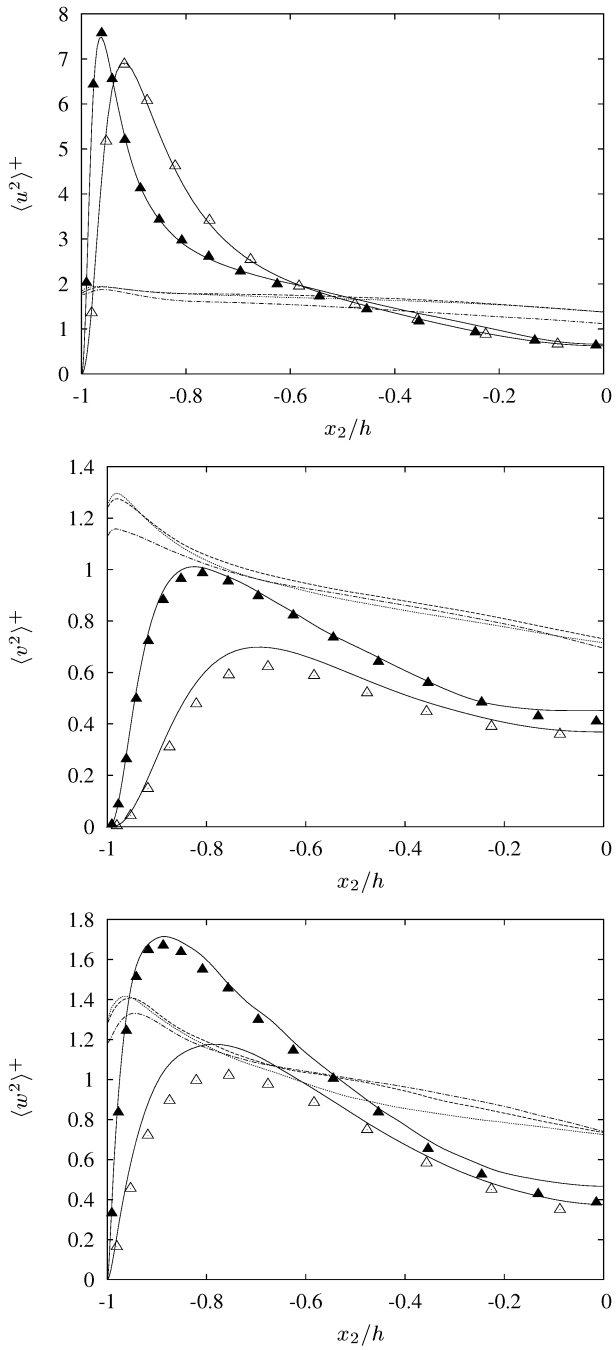

Figure 6: Turbulent intensities in wall units. Smooth channel: ——— Kim *et al.* (1987), Moser *et al.* (1999), symbols present simulations. Empty symbols $Re = 4200$, filled $Re = 10400$. Roughness $w/k = 9$, —·— $Re = 4200$, – – – – $Re = 10400$, ····· $Re = 18000$.

larger than over a smooth wall and even far from the wall its value is about twice that of a smooth wall. The normal wall velocity is the quantity most affected by the rough wall. Orlandi *et al.* (2003) showed that the salient characteristic of rough wall flows is the presence of a non-zero wall-normal normal velocity distribution at the interface between the roughness cavities and the external flow. Near the wall $\langle w^2\rangle^+$ increases

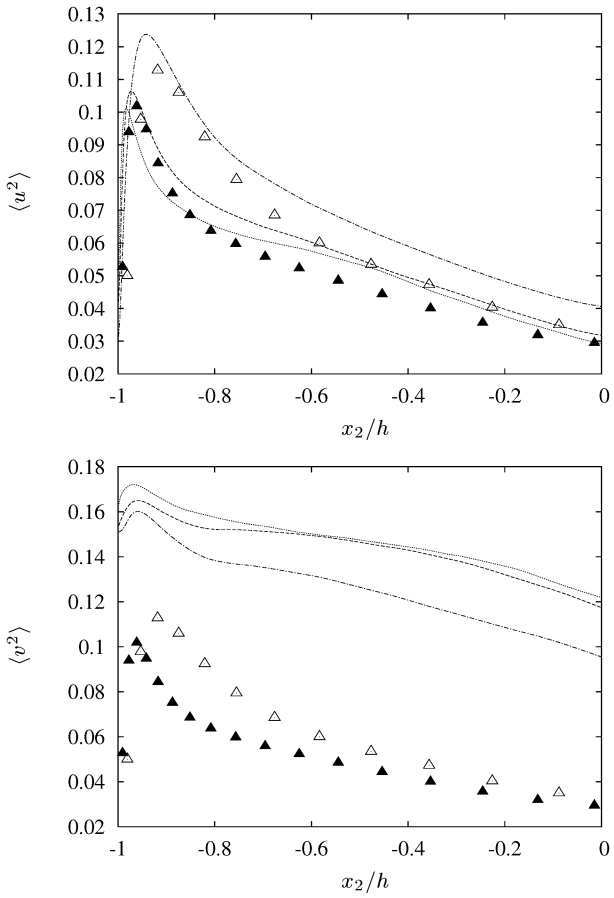

Figure 7: Turbulent intensity of the streamwise velocity. Symbols, smooth channel present simulation. Empty symbols $Re = 4200$, filled $Re = 10400$. Top $w/k = 1$, bottom $w/k = 9$; —·— $Re = 4200$, – – – – $Re = 10400$, ····· $Re = 18000$.

with respect to the smooth wall at low Reynolds number ($Re_\tau = 180$) but decreases with respect to the smooth channel at $Re_\tau = 380$. Far from the wall, at about $x_2/h = -0.4$ ($6k$ above the roughness crests plane) $\langle w^2\rangle^+$ is larger than that relative to the smooth wall at both Reynolds numbers. With respect to the smooth wall, peaks of all the turbulent intensities are shifted towards the roughness crest plane. The dependence of the turbulent intensities for $w/k = 9$ on the Reynolds number is weak. Regardless of the differences in k^+ and ΔU^+ turbulent intensities agree closely throughout the channel. In particular, the distributions for $Re = 10400$ and 18000 overlap, while those for $Re = 4200$ near the wall are slightly different. Hanjalic & Launder (1972) performed an experiment at higher Reynolds numbers in a channel with square bar roughness. In agreement with the present results, they found that the turbulent intensities, scaled in wall units, do not depend on the Reynolds number. The same turbulent intensities correspond to 3 different roughness functions, which may be interpreted as further evidence for the inadequacy of ΔU^+ in characterizing the effect of the roughness. The distributions of all the turbulent intensities never overlap those for the smooth channel even at the centreline, which is $10k$ above the roughness crest plane. The largest differences are found, as expected, for the wall-normal turbulent intensity. In the light

of the present findings the results obtained by Krogstad and Antonia (1999) are not surprising. The authors considered two different rough surfaces with the same roughness function and found significant differences in $\langle v^2 \rangle$ in the outer layer. Since the roughness function is not a physical meaningful signature of the particular geometry considered, differences between the turbulent intensities are expected. The fact that these differences extend even into the outer layer seems to be confirmed by the present simulations given that at a distance of $10k$ above the roughness crest plane, $\langle v^2 \rangle^+$ is about twice than that on a smooth wall. However, we are aware that our ratio h/k may be too small, and a further validation is required with smaller roughness elements (Jimenez 2004).

For smaller values of w/k, the frictional drag increases its importance respect to the form drag. A larger Reynolds number dependence is expected, and in fact, close to the wall, the turbulent intensities vary more than for $w/k = 9$ (fig. 8). The distributions are similar to those for $w/k = 9$, but the turbulent intensities are closer to those of the smooth channel. In particular, $\langle u^2 \rangle^+$ at about $x_2/h = -0.2$ coincides with that of the smooth channel and the wall-normal turbulent intensities at the centreline is only 50% larger than that of the smooth channel. However, small perturbations, such as those caused by the square cavities, produce differences in turbulent intensities which extend to more than $10k$ above the roughness crest plane.

Since relative to a smooth channel, $\langle u^2 \rangle^+$ decreases and $\langle v^2 \rangle^+$ increases, it can be concluded that roughness leads to an improved global isotropy independently of the Reynolds number.

CONCLUSIONS

Direct Numerical Simulations of turbulent channel flows with roughness on the bottom wall have been performed for $w/k = 1$ and 9 at three different Reynolds numbers. The effect of the Reynolds number is weak especially for $w/k = 9$ where the form drag is dominant. This provides strong motivation for using DNS data at only moderate Reynolds numbers (say $Re \simeq 10.000$) to shed light into flows over rough walls. It has been shown that the roughness function, to a large extent, reflect the choice of origin for y. For $w/k = 1$, the roughness function does not depend on k^+ because the origin is at the roughness crest plane. For $w/k = 9$, the turbulent intensities for 3 different values of ΔU^+ (corresponding to 3 Reynolds numbers) are in reasonable agreement with each other. This result highlights the inadequacy of using ΔU^+ for characterizing the effect of the roughness.

Relative to a smooth wall, the roughness considered here results in an improvement in the level of isotropy independently of the Reynolds number.

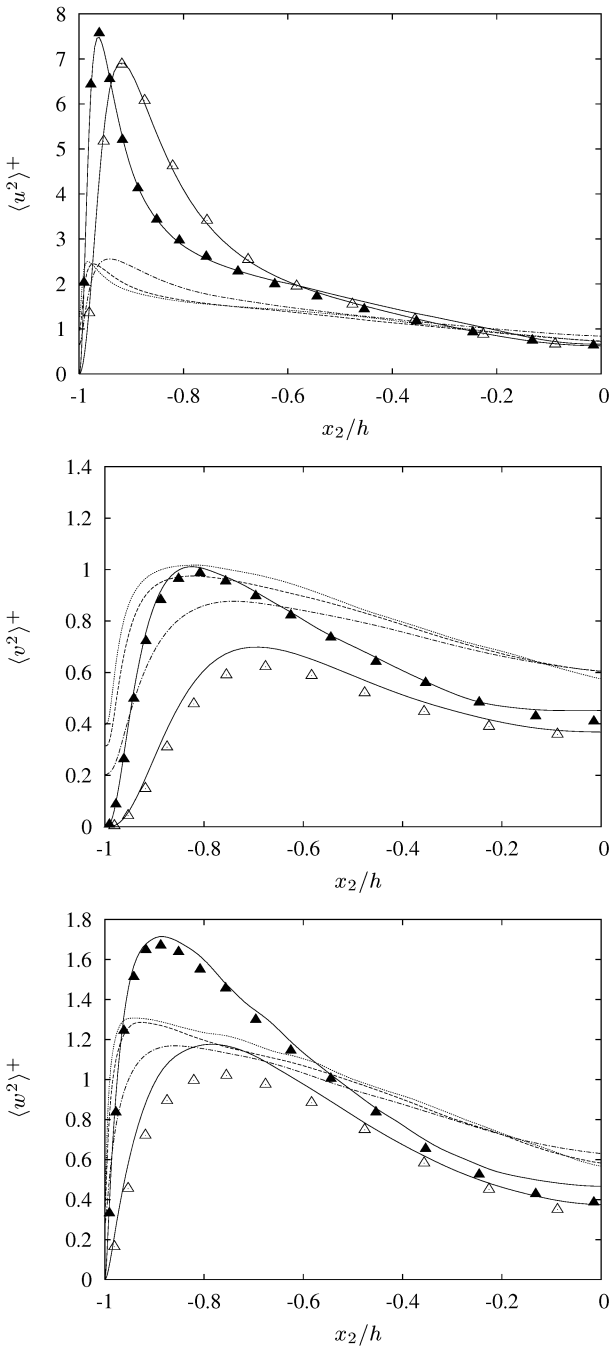

Figure 8: Turbulent intensities in wall units. Smooth channel: ——— Kim *et al.* (1987), Moser *et al.* (1999), symbols present simulations. Empty symbols $Re = 4200$, filled $Re = 10400$. Roughness $w/k = 1$, —·— $Re = 4200$, - - - - $Re = 10400$, ····· $Re = 18000$.

ACKNOWLEDGMENTS

This research has been supported by MURST 60 % and Australian Research Council.

REFERENCES

Ashrafian A., Andersson H. I. & Manhart M. (2004). DNS of turbulent flow in a rod-roughened channel. *I. J. of Heat and Fluid Flow*, **25**, Issue 3, 373-383.

Bakken O.M. & Krogstad P. A. (2003). Stress measurements in a rough wall channel flow using variable angle method of calibration for X–probes.Proceedings of the TSFP3, Sendai, Japan. N. Kasagi, J. K. Eaton, R. Friedrich, J. A. C. Humphrey, M. A. Leschziner, T. Miyauchi. **Vol I**, 105–111.

Bandyopadhyay, P.R. (1987). Rough–wall turbulent boundary layers in the transition regime. *J. Fluid Mech.* **180**, pp.231–266.

Bhaganagar, K., Kim, J. & Coleman, G. 2004. Effect of roughness on wall-bounded turbulence *Flow Turbulence and Combustion* **72** ,463–492.

Cui J., Virendra C. Patel & Ching-Long Lin (2003). Large–eddy simulation of turbulent flow in a channel with rib roughness. *Int. J. of Heat and Fluid Flow* **24** 372–388.

Hanjalic & Launder (1972). Fully developed asymmetric flow in plane channel. *J.* Fluid Mech. **51**, 301–335.

Kim, J. , Moin, P. & Moser, R. (1987). Turbulence statistics in fully developed channel flow at low Reynolds number. *J. Fluid Mech.* **177**, 133–166.

Krogstad, P.-Å. & Antonia, R. A. 1999. Surface roughness effects in turbulent boundary layers. *Expts. Fluids* **27**, 450–460.

Jackson, P.S. (1981). On the displacement height in the logarithmic profile. *J. Fluid Mech.* **111**, 15–25.

Jiménez, J. 2004. Turbulent flows over rough walls *Ann. Review of Fluid Mech.* **36** , 173–196.

Leonardi, S., Orlandi, P., Smalley, R.J., Djenidi, L. & Antonia, R.A. (2003). Direct numerical simulations of turbulent channel flow with transverse square bars on one wall. *J. Fluid Mech.* **491**, 229-238.

Leonardi S., Orlandi P. & Antonia R.A. (2005) A method for determining the frictional velocity in a turbulent channel flow with roughness on the bottom wall. *Exps. Fluids* accepted for publication.

Moser R.D., Kim J. & Mansour N.N. (1999). *Phys. Fluids* **11**, 943-945.

Orlandi, P. (2000) Fluid flow phenomena, a numerical toolkit. *Kluwer Academic Publishers.*

Orlandi P., Leonardi S., Tuzi R. & Antonia A.R. 2003. DNS of turbulent channel flow with wall velocity disturbances *Phys. Fluids* **15** , 3497–3600.

Perry, A. E., Schofield, W. H. & Joubert, P. N. 1969. Rough wall turbulent boundary layers. *J. Fluid Mech.* **37**, 383–413.

Smalley R.J., Leonardi S., Antonia R.A., Djenidi L. & Orlandi P. (2002). Reynolds stress anisotropy of turbulent rough wall layers.*Exps. Fluids* **33** 31–37.